ARTICLE

BIOTECHNOLOGY and BIOENGINEERING

Peak Antibody Production is Associated With Increased Oxidative Metabolism in an Industrially Relevant Fed-Batch CHO Cell Culture

Neil Templeton,[1] Jason Dean,[2] Pranhitha Reddy,[2] Jamey D. Young[1]

[1]Chemical and Biomolecular Engineering, Vanderbilt University, PMB 351604, Nashville, Tennessee 37235; telephone: +615-343-4253; fax: +615-343-7951; e-mail: j.d.young@vanderbilt.edu

[2]Amgen, Cell Sciences and Technology, Seattle, Washington 98119

ABSTRACT: Cell metabolism can vary considerably over the course of a typical fed-batch antibody production process. However, the intracellular pathway alterations associated with various phases of growth and antibody production have yet to be fully elucidated using industrially relevant production hosts. Therefore, we performed ^{13}C labeling experiments and metabolic flux analysis (MFA) to characterize CHO cell metabolism during four separate phases of a fed-batch culture designed to closely represent industrial process conditions. First, we found that peak specific growth rate was associated with high lactate production and minimal TCA cycling. Conversely, we found that lactate metabolism switched from net production to net consumption as the culture transitioned from peak growth to peak antibody production. During the peak antibody production phase, energy was primarily generated through oxidative phosphorylation, which was also associated with elevated oxidative pentose phosphate pathway (oxPPP) activity. Interestingly, as TCA cycling and antibody production reached their peaks, specific growth rate continued to diminish as the culture entered stationary phase. However, TCA cycling and oxPPP activity remained high even as viable cell density began to decline. Overall, we found that a highly oxidative state of metabolism corresponded with peak antibody production, whereas peak cell growth was characterized by a highly glycolytic metabolic state.

Biotechnol. Bioeng. 2013;110: 2013–2024.

KEYWORDS: metabolic flux analysis (MFA); Chinese hamster ovary (CHO); fed-batch; lactate switch; antibody production; aerobic glycolysis

Introduction

Chinese hamster ovary (CHO) cells are currently the preferred host for recombinant antibody production, supplying 60–70% of the nearly $100 billion global biotherapeutics market (Ahn and Antoniewicz, 2012). Production of recombinant antibodies is energetically costly to the host cell, requiring roughly three molecules of ATP to synthesize just one peptide bond (Seth et al., 2006). A highly producing cell line can potentially generate 40 pg of antibody each day (Seth et al., 2006), representing up to 20% of the cell's total intracellular protein (Nyberg et al., 1999). Despite these energy and material demands, mammalian cell lines often exhibit an inefficient glycolytic state of metabolism involving rapid conversion of glucose to lactate even in the presence of abundant oxygen (Ahn and Antoniewicz, 2012). Furthermore, increased consumption of glutamine is also exhibited by many continuous cell lines, but much of the nitrogen provided by this substrate is subsequently lost to the production of ammonia and alanine (Hansen and Emborg, 1994). While minimizing wasteful byproduct accumulation has been a goal of the mammalian biotech industry for over 25 years, it still remains an unresolved issue. Furthermore, many production cultures will shift from net production to net consumption of these byproducts during the bioprocess run (Nolan and Lee, 2011); however, the regulatory mechanisms that control this switch are still poorly understood.

Fed-batch bioreactors are the most common system of monoclonal antibody production used today (Birch and Racher, 2006). Fed-batch reactors have a key advantage over other systems, such as perfusion culture, because a higher final product titer can be achieved. This limits the cost associated with downstream processing and purification (Altamirano et al., 2004). One challenge of fed-batch designs is that culture metabolism changes substantially over the course of the production run. This can be attributed to changing nutrient availability and cell density that give rise to transitions between distinct growth phases

The authors declared they have no conflicts of interest.
Correspondence to: J. D. Young
Contract grant sponsor: Amgen, Inc.
Contract grant number: 2010529686
Additional supporting information may be found in the online version of this article.
Received 26 July 2012; Revision received 11 January 2013; Accepted 22 January 2013
Accepted manuscript online 4 February 2013;
Article first published online 4 March 2013 in Wiley Online Library (http://onlinelibrary.wiley.com/doi/10.1002/bit.24858/abstract)
DOI 10.1002/bit.24858

(i.e., exponential, stationary, and decline). Furthermore, concentrations of lactate, ammonia, and other waste products can accumulate during early growth phases to concentrations that inhibit cell growth and antibody production and impact protein glycosylation during later phases (Wlaschin et al., 2006). Byproduct accumulation can also lead to excessive increases in osmolarity, especially when online base addition is used to control pH (Omasa et al., 1992). To mitigate these effects, much prior work has examined the impacts of process parameters such as pH, temperature, CO_2, and osmolarity on process performance (Birch and Racher, 2006). Information from these studies has been used to design optimal media formulations and feeding strategies that reduce byproduct accumulation by limiting the supply of glucose, glutamine, or other nutrients to the culture (Altamirano et al., 2004, 2006). Further work has examined metabolic engineering of CHO cells to enhance pyruvate entry into mitochondria by over-expressing the pyruvate carboxylase (PC) enzyme (Fogolín et al., 2004) or to resist cell toxicity by overexpressing various anti-apoptotic proteins (Dorai et al., 2009).

While previous studies have led to substantial improvements in bioprocess rates and titers, the ability to precisely quantify cell metabolism throughout multiple growth phases is essential to further understand and optimize the industrial fed-batch production process. Metabolic flux analysis (MFA) provides a powerful approach to map intracellular carbon flows of cultured cells and thereby elucidate the functional behavior of entire biochemical networks, as opposed to studying individual reactions or nodes in isolation (Sauer, 2006). MFA has been applied to a variety of bioprocess applications, including optimization of medium composition and feeding strategies (Xing et al., 2011), data reconciliation and error analysis of measured rates (Goudar et al., 2009), and to draw comparisons between the metabolism of CHO cells and other continuous cell lines (Quek et al., 2010). Most prior MFA studies on CHO cells have relied on classical metabolite balancing to estimate fluxes without the use of ^{13}C tracers (reviewed by Ahn and Antoniewicz, 2012). This necessitates the use of simplified network models and ad hoc assumptions to determine fluxes based on measured nutrient uptake and product secretion rates. Alternative approaches have also been developed to calculate upper and lower flux bounds using large-scale stoichiometric models without attempting to solve explicitly for the unidentifiable fluxes (Quek et al., 2010). To our knowledge, only three prior MFA studies have applied ^{13}C tracing of CHO cell cultures to fully resolve fluxes through parallel and cyclic reaction pathways, (Ahn and Antoniewicz, 2011; Goudar et al., 2010; Sengupta et al., 2011). However, only Sengupta et al. (2011) applied ^{13}C-MFA to examine fed-batch culture of an antibody-secreting CHO cell line, and their work was limited to the late stationary growth phase. On the other hand, Ahn and Antoniewicz (2011) applied ^{13}C-MFA to compare flux maps between exponential and stationary growth phases of a fed-batch CHO culture, but their work examined an adherent CHO-K1 line that did not express recombinant antibody. Therefore, comprehensive understanding of CHO cell physiology based on ^{13}C-MFA is still lacking, especially in regards to how CHO metabolism adapts to changing growth and antibody secretion rates over the course of an industrially relevant fed-batch bioprocess.

In this study, we have performed ^{13}C labeling experiments and MFA to characterize cell metabolism throughout four separate phases of an industrial fed-batch process. A small-scale culture system with a highly productive (HP) recombinant antibody-producing CHO cell line was used to represent a typical manufacturing-scale serum-free process. Using MFA, we initially observed that the demands of peak growth were met by a highly glycolytic state of metabolism, but as time progressed the culture shifted to an increasingly oxidative state that coincided with peak antibody production. All major pathways of central metabolism were considered in our analysis, including glycolysis, pentose phosphate pathway, TCA cycle, and various cataplerotic and anaplerotic pathways. In a complementary study, both the expression and activity of several relevant enzymes within these pathways were verified (Dean and Reddy, 2013). To our knowledge, this is the first time that MFA has been applied to characterize multiple phases of an industrial antibody-producing fed-batch CHO cell bioprocess.

Methods

Cell Culture

A highly-productive (HP) CHO cell line was generated by transfecting plasmid DNA containing mAb light chain and heavy chain into a dihydrofolate reductase-deficient CHO cell line adapted to suspension and serum-free growth media. Prior to the experiment, these cell lines were passaged every 3 or 4 days at a density of 3×10^5 cells/mL in peptone- and methotrexate-containing growth media in a humidified incubator maintained at 36°C and 5% CO_2 with shaking at 150 RPM. This temperature was held constant throughout the experiment.

To initiate the fed-batch experiment, the culture was inoculated into a chemically defined production media at a viable cell density of approximately 5×10^5 cells/mL. Fed-batch cultures were grown using 25 mL of culture volume in 125 mL shake flasks or 3.6 mL in 24 deep-well plates in humidified incubators maintained at 36°C and 5% CO_2 with shaking at either 150 RPM (125 mL shake flask) or 220 RPM (24 deep-well plate). The production was carried out for 10 days by feeding 5%, 5%, and 9% of the initial culture volume of a chemically defined concentrated amino acid feed on Days 3, 6, and 8. On Days 3, 6, and 8, glucose concentrations were adjusted to 55.6 mM (10 g/L). This feeding schedule was chosen to represent a typical fed-batch process used at Amgen. Due to the fact that metabolic steady state was perturbed by media additions, a minimum of 48 h were allowed for

metabolic quasi-steady-state to be re-established before the culture was sampled and cold-quenched prior to metabolite extraction and GC–MS analysis.

Determination of Nutrient Uptake and Product Excretion Rates

Extracellular media samples were taken at multiple times throughout the experiment. Glucose and lactate concentrations were determined by enzymatic assay using an automated poly-chem instrument (Polymedco, Cortlandt Manor, NY). Viable cell density (VCD) and percentage viability was determined by using a ViCell (Beckman Coulter, Fullerton, CA). Antibody titer was determined by high performance liquid chromatography (HPLC) using a Protein-A column. Amino acid concentration was determined by HPLC using a 6-aminoquinolyl-*N*-hydroxysuccinimidyl carbamate derivatization method. Extracellular pyruvate concentrations were determined using an organic acid Aminex HPX-87H column (Biorad, Hercules, CA) as previously described (Dean et al., 2009).

The specific growth rate, specific death rate, and gross growth rates were determined by the following equations:

$$\frac{dX}{dt} = \mu_{net} X,$$

$$\frac{dX_d}{dt} = k_d X,$$

$$\mu_{net} = \mu_{gross} - k_d$$

where X represents viable cell density, X_d represents dead cell density, μ_{net} represents net specific growth rate, k_d represents specific death rate, μ_{gross} represents gross specific growth rate, and t represents time. Cell specific rates of nutrient uptake and product excretion were determined using the following equation:

$$\frac{dC_i}{dt} = -k_i C_i + q_i X,$$

where C_i represents concentration, q_i represents cell specific production rate (or consumption rate if negative), and k_i represents the first-order degradation rate of the ith biochemical component in the extracellular medium. Degradation rate for most metabolites was negligible, with the exception of glutamine. The spontaneous rate of glutamine degradation, calculated in the absence of cells at incubation conditions, was found to be 0.087 day^{-1}. This rate of degradation was significant (relative to cell specific uptake), as has been reported previously in literature (Ozturk and Palsson, 1990). All specific rates were calculated using the method of Glacken et al. (1988), where regression analysis was applied to estimate parameters in the proceeding equations using extracellular time course measurements.

Intracellular Redox Measurements

NADPH/$NADP^+$, and GSH/GSSG (reduced/oxidized glutathione) measurements were performed on 2×10^6 cells collected from 125 mL fed-batch production cultures using enzymatic assay kits according to the manufacturer's instructions (Abcam, Cambridge, MA). NADH/NAD^+ measurements were performed on 1×10^6 cells collected from 125 mL fed-batch production cultures using an enzymatic assay kit (Abcam, Cambridge, MA).

Steady-State Isotope Labeling Experiments

Steady-state labeling was achieved in free intracellular metabolites by feeding labeled substrates for a minimum of 48 h prior to sampling, which has been previously shown to be sufficient for most free metabolites to achieve isotopic equilibrium in CHO cell cultures (Deshpande et al., 2009). Because the metabolism of the culture was changing gradually over time, the measured labeling represents a quasi-steady state condition based on the assumption that the dynamics of isotope labeling occur more rapidly than the metabolic transients. Some bias may be introduced into the MFA results to the extent that this assumption is not strictly satisfied; however, we expect that our key conclusions are robust to minor violations of this assumption.

Multiple parallel isotope labeling experiments were performed to enable flux analysis of each growth phase

Table I. Fed-batch schedule for isotope labeling experiments.

Day	0	1	2	3	4	5	6	7	8	9	10
Day 0–3	Seed			Quench							
Day 3–5	Seed			Feed		Quench					
Day 6–8	Seed			Feed			Feed		Quench		
Day 8–10	Seed			Feed			Feed		Feed		Quench

Parallel ^{13}C-labeling experiments were carried out to enable flux analysis of each growth phase. The lightly shaded section indicates when the culture was exposed to ^{13}C labeled substrates. The culture was regularly fed an optimized nutrient-rich complex on the days indicated by "Feed." Fields labeled as "Quench" indicate the times when the culture was harvested for intracellular metabolite analysis. The darkly shaded section of the chart represents the post-experiment period. The culture had already been quenched and terminated prior to that time.

(Table I). In the case of the Day 0–3 experiment, 72 h were allowed to achieve isotopic steady state. Two separate tracer experiments were conducted in parallel for the Day 0–3 time-interval. In the first experiment, a cocktail of glucose tracers was administered, composed of 50% [1,2-$^{13}C_2$] glucose, 30% [U–$^{13}C_6$] glucose, and 20% [1-^{13}C] glucose. [U–$^{13}C_6$] glucose has been previously shown to be an effective tracer for estimating TCA cycle fluxes, while [1,2-$^{13}C_2$] glucose and [1-^{13}C] glucose provide information on the branch ratio between glycolysis and oxPPP (Metallo et al., 2009). The tracer mixture was optimized using the approach of Möllney et al. (1999). In the second experiment, [U–$^{15}N_2$, U–$^{13}C_5$] glutamine was used to achieve increased labeling of TCA cycle intermediates, since a large fraction of the glucose substrate was diverted to lactate during the initial Day 0–3 time-interval. The labeling data from both parallel experiments were simultaneously fitted to the same isotopomer model in order to estimate metabolic fluxes. The three other fed-batch phases of interest for this study (Day 3–5, Day 6–8, and Day 8–10) used 100% [U–^{13}C] glucose as the labeled substrate. This tracer was chosen in order to maximize identifiably of TCA cycle and amphibolic mitochondrial pathway fluxes. In these latter experiments, labeling was allowed to equilibrate for 48 h prior to sampling.

Metabolite Cold-Quenching and Extraction

Due to the fact that some intracellular metabolites are turned over on a short time scale, rapid cold-quenching is necessary to capture an accurate snapshot of intracellular metabolism (Dietmair et al., 2010). With this in mind, an ammonium bicarbonate (AMBIC) cold-quench was performed (Sellick et al., 2009). Here, AMBIC makes up 0.85% (w/v) of the aqueous portion of the quenching solution, which is a 60/40 mixture of methanol/AMBIC pre-cooled to −40°C. At each sample time point, an aliquot of culture medium containing approximately 10 million viable cells was drawn into a syringe and rapidly sprayed into the quenching solution. Following the cold-quench, metabolite extraction was performed using the Folch method (Folch et al., 1957).

Derivatization and Gas Chromatography Mass Spectrometry (GC–MS) Analysis

Derivatization for GC–MS was initiated by dissolving evaporated metabolite extracts in 50 μL of methoxyamine reagent (MOX; Pierce, Rockford, IL). Following 30 min of sonication at room temperature, the sample was incubated for 90 min at 40°C. Then, 70 μL of MTBSTFA + 1% TBDMCS (Pierce) in pyridine was added, and the solution was incubated for 30 min at 70°C. Lastly, the samples were centrifuged at 14,000 RPM to remove any solid precipitates.

Derivatized extracts were analyzed with a HP5-MS capillary column (30 m × 0.25 mm i.d. × 0.25 μm; Agilent J&W Scientific) installed in an Agilent 7890A gas chromatograph (GC). The injection volume was 1 μL and all samples were run in split mode (50:1) with an inlet temperature of 270°C. Helium flow rate was set to 1 mL/min. The GC oven temperature was held at 80°C for 5 min, ramped at 20°–140°C/min and held for 0 min, and ramped once more at 4°–280°C/min and held for 5 min. Mass spectra were obtained using scan mode over the range of 100–500 m/z. Raw ion chromatograms were integrated using a custom MATLAB program that applied consistent integration bounds and baseline correction to each fragment ion (Antoniewicz et al., 2007).

Isotopomer Network Model

A reaction network was generated to accurately represent the central metabolism of CHO cells. This network consisted of glycolysis, TCA cycle, pentose phosphate pathway, multiple cataplerotic and anaplerotic reactions, and both catabolism and anabolism of amino acids. ATP and NAD(P)H were not included in the stoichiometric balances, as they have been shown to produce inconsistent results in mammalian cell cultures (Bonarius et al., 1998). In total, there were 71 reactions that made up this network with 23 extracellular metabolites and two macromolecular products, antibody and biomass. Further details of the reaction network are provided in the Supplementary Materials.

Biomass and Antibody Demands

In order to develop an accurate biomass equation, the dry weight of the HP cell line was determined to be approximately 329 pg per cell on average. This was calculated after drying and weighing a known amount of cells in a plastic petri dish in a non-humidified 37°C incubator. The composition of the cell mass was based upon previous work available in literature for hybridoma cells (Sheikh et al., 2005). The included contents of the dry cell mass for the biomass equation were protein, glycogen, lipids, and nucleotides. Each macromolecule was stoichiometrically decomposed into its independent precursor building blocks. Protein composition was based upon the relative amount of each amino acid. Each glycogen monomer was assumed to be composed of one G6P. Lipids were broken down into cholesterol, phosphatidylcholine, phosphatidylethanolamine, phosphatidylinositol, phosphatidylserine, phosphatidylglycerol, diphosphatidylglycerol, and sphingomyelin. Biosynthesis of nucleotides was also considered, based on the demands of both DNA and RNA. The biosynthetic demands for recombinant antibody production were based solely upon its amino acid composition. For further information about both the antibody and biomass equations, refer to the Supplementary Materials.

Table II. Key characteristics of each fed-batch phase.

Time	μ_{Gross}	k_d	Phase	Key characteristic(s)
Day 0–3	0.70 ± 0.02	0.013 ± 0.003	Early Exponential	Peak growth/glycolytic flux
Day 3–5	0.59 ± 0.03	0.014 ± 0.001	Late Exponential	Peak PPP flux
Day 6–8	0.29 ± 0.03	0.045 ± 0.003	Stationary	Peak antibody production/TCA cycling
Day 8–10	0.09 ± 0.06	0.107 ± 0.014	Decline	Loss of viability/PPP and TCA maintained

Standard error of the mean is reported for gross specific growth rates (μ_{gross}) and specific death rates (k_d). The difference between these two rates gives the net specific growth rate. Reported units are inverse days.

Flux Determination and Statistical Analysis

Isotopic steady-state MFA was applied based on both the measured cell specific uptake and excretion rates and the measured intracellular isotopomer abundances (Antoniewicz et al., 2007). This approach involved solving an inverse problem where metabolic fluxes were determined by least-squares regression of experimental measurements using the isotopomer network model. Flux estimations were repeated a minimum of 100 times from a randomized initial guess to ensure the global solution was obtained. A chi-square statistical test was used to assess goodness-of-fit and a sensitivity analysis was performed to determine 95% confidence intervals associated with the reported flux values (Antoniewicz et al., 2006).

Results and Discussion

Fed-Batch Growth

The HP CHO cell line reached a peak viable cell density of approximately 20 million cells/mL, maintained greater than 80% cell viability throughout the culture, and produced a final antibody titer of greater than 3 g/L over the course of a 10-day fed-batch culture. The culture was fed on days 3, 6, and 8, which dictated the timing and duration of the separate growth phases included in our subsequent analysis (Table II).

Stoichiometric Analysis

A stoichiometric analysis was performed upon each separate growth phase shown in Table II, accounting for all major incoming and outgoing carbon fluxes. Glucose and amino acids supplied essentially all of the incoming carbon flux to the culture, with pyruvate serving as an additional carbon source during the initial growth phase. While glutamine was the most important amino acid during Early Exponential phase, other amino acids became important in later growth phases once glutamine had been depleted from the medium. During Early and Late Exponential phases, much of the carbon consumed was used for biomass production (Fig. 1A), with the balance largely converted to lactate (Fig. 2). At later phases, biomass synthesis was diminished and antibody production became a major component of the biosynthetic demand. Furthermore, lactate metabolism switched from net production to net consumption as the culture entered Stationary phase. The overall rate of carbon consumption fell gradually at each fed-batch stage (Fig. 3), which can be largely attributed to the falling specific growth rate (Fig. 1A).

Nutrient Consumption

When glutamine and glucose carbon fluxes are summed, they comprise approximately 70% of the total incoming extracellular flux during Early Exponential phase (Fig. 2). Glutaminolysis was substantially reduced following this phase, but glucose consumption remained relatively high throughout all growth phases and never dropped below 50% of its initial rate (Fig. 1A). The rate of glutamine uptake during Early Exponential phase greatly exceeded the biosynthetic demand for biomass or antibody production. The excess glutamine consumed was catabolized to provide energy, as has been observed before (DeBerardinis et al., 2007). Experiments using [U–$^{13}C_6$] and [U–$^{15}N_2$] glutamine showed that glutamine was largely converted to alanine and lactate (Dean and Reddy, 2013). The total amino acid contribution to incoming carbon flux was considerable over the entire fed-batch process (between 30% and 50% of total carbon) with the uptake of other amino acids increasing after glutamine was depleted (Fig. 2). In particular, asparagine represented 5% of the incoming carbon flux during Early Exponential and 8% during Stationary phase.

Product Formation

Antibody production was at its minimum during Early Exponential phase (only 3% of output carbon flux), but production rate more than doubled during Stationary phase (15% of output carbon flux) (Figs. 1B and 2). Conversely, biomass production went from being the largest single outgoing flux at Early Exponential phase to being almost negligible during Decline phase. In spite of this, we observed that antibody demand for incoming carbon flux was less than biomass demand in most phases, with the only exception perhaps being the Decline phase. Following a similar pattern as biomass production, lactate production represented over 35% of the total outgoing carbon flux during Early Exponential phase. It was substantially reduced during Late Exponential phase, and it reversed direction during Stationary phase. The production of several amino acids such as glutamate, alanine, and aspartate was also

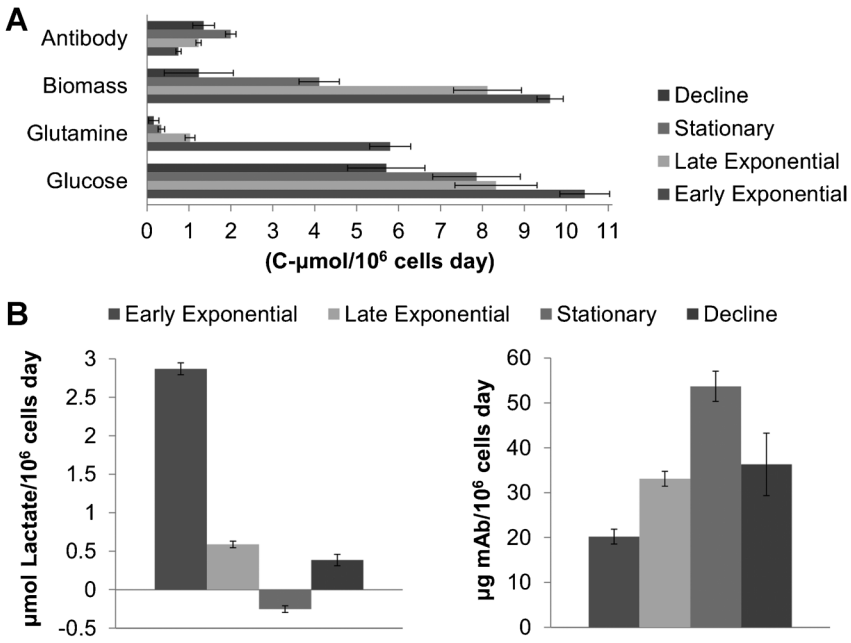

Figure 1. Major nutrient uptake and product formation rates. **A**: Key biosynthetic and nutrient uptake rates expressed on a carbon basis. Error bars indicate the standard error of the regressed rate parameters. **B**: Specific lactate and antibody fluxes during each phase.

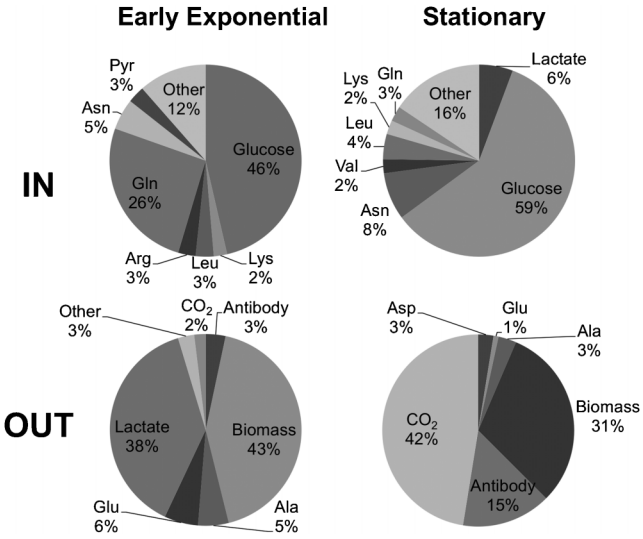

Figure 2. Stoichiometric analyses of measured nutrient uptake and product formation rates. Fractional contributions are expressed on a carbon basis and were calculated from direct measurements of extracellular medium composition over time, with the exception of carbon dioxide. The CO_2 contribution was estimated from the difference between measured incoming and outgoing carbon fluxes, as needed to complete the mass balance. The estimated CO_2 production rates were within the expected range based on experimentally determined rates of oxygen consumption and respiratory quotient obtained from independent bioreactor studies (Follstad, 2012, personal communication). "Other" indicates the sum of several amino acids that make minor contributions to overall carbon flux.

observed, where glutamate excretion was associated with increased glutamine uptake and aspartate excretion was associated with increased asparagine uptake.

Metabolic Flux Analysis

To further investigate the intracellular pathway alterations associated with the various growth phases of this fed-batch process, isotope-labeling experiments were performed to enable comprehensive metabolic flux analysis. The MFA results for each growth phase are summarized in the flux maps shown in Figure 4. In the following, we discuss the key

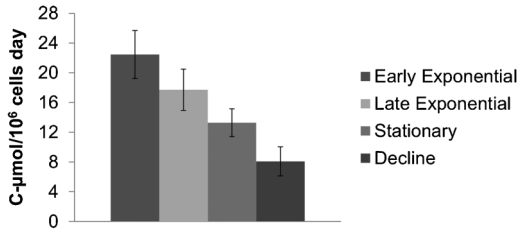

Figure 3. Total incoming carbon flux during each fed-batch phase. The contributions of all measured incoming carbon sources have been summed. Error bars indicate the propagated standard error.

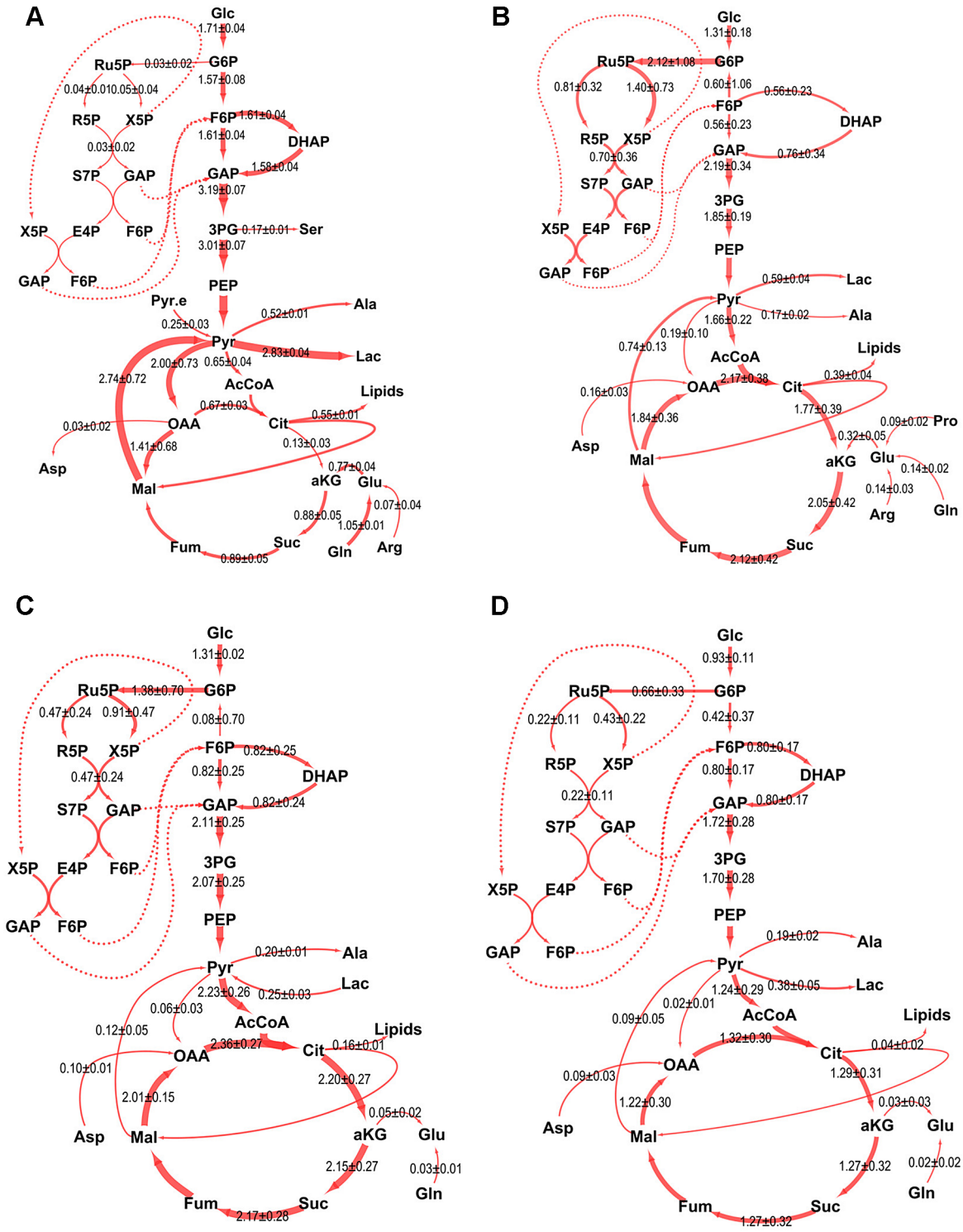

Figure 4. Metabolic flux maps for all growth phases. Reported fluxes (μmol/10^6 cells day) are the median of the 95% confidence interval, with associated standard errors shown. Arrow thickness is scaled proportional to the flux value. Dotted lines indicate transfer of identical metabolites involved in separate pathways, and are not actual fluxes included in the model. The flux maps were generated using Cytoscape, a freely available software (Smoot et al., 2011). **A**: Early Exponential; **B**: Late Exponential; **C**: Stationary; and **D**: Decline.

features of each major pathway and how the functional state of the network varies over time. Here, it is important to consider these results within the context of the overall trend of decreasing total carbon uptake depicted in Figure 3.

Additionally, it is important to recognize that these results are representative of one cell line grown under one set of experimental conditions, and that metabolic fluxes can depend strongly on the growth conditions chosen for the

study (Sengupta and Morgan, 2010). Our interest here was to determine how cell metabolism adapts over the course of a typical fed-batch process, with the cell line and media conditions selected to be representative of an industrial process used at Amgen.

Glycolysis

Growth was at its maximum during Early Exponential phase, yet much of the incoming carbon from glucose was converted to lactate and alanine. Minimal flux was diverted into the oxidative pentose phosphate pathway (oxPPP), as over 90% of the incoming glucose was metabolized directly into glycolysis. High glycolytic activity, and specifically lactate production, has been previously associated with increased growth of mammalian cells. As stated in previous work (Li et al., 2012), one hypothesis is that lactate production is an adaptation to increase the availability of biosynthetic precursors needed to generate biomass (DeBerardinis et al., 2008; Shaw, 2006; Vander Heiden et al., 2009). In contrast to Early Exponential phase, lactate production was substantially reduced in Late Exponential phase and even reversed itself during Stationary phase. Whereas lactate represented over 35% of the total *outgoing* carbon flux during Early Exponential phase, it accounted for 6% of the *incoming* carbon flux during Stationary phase. On the other hand, glucose consumption and overall glycolytic flux decreased by roughly one-third following Early Exponential phase and remained relatively constant throughout Late Exponential and Stationary phases.

Pentose Phosphate Pathway

Although essentially non-existent during Early Exponential phase, oxPPP flux was substantial during all later growth phases. Even during Decline phase, when total incoming carbon flux was reduced by 65%, glucose-6-phosphate dehydrogenase (G6PDH) flux was still much larger than during Early Exponential phase. Further verification of changing oxPPP activity was provided in a parallel [1,2-$^{13}C_2$]glucose study where only M + 2 lactate mass isotopomers were observed during Early Exponential phase but substantial M + 1 labeling was observed during Stationary phase (Dean and Reddy, 2013). Other studies have also observed significant G6PDH flux during the stationary phase of a fed-batch CHO cell culture (Sengupta and Morgan, 2010), where nearly all of the incoming glucose was diverted to the oxPPP. In our work, all of the incoming glucose was diverted to the oxPPP during both Late Exponential and Stationary phases, which also corresponded with peak antibody production. In fact, G6PDH flux was greater than hexokinase (HK) during these periods, implying that oxPPP was operating in a cyclic mode with net conversion of F6P to G6P.

Minimal oxPPP activity during exponential growth has been reported in other CHO cell MFA studies (Ahn and Antoniewicz, 2011). This does however raise the important question of where the necessary NADPH for growth and maintenance of cellular redox was derived during Early Exponential phase. It has been estimated that 1–2 moles of NADPH are required per mole of acetyl-CoA incorporated into lipid (Xie and Wang, 1996). ATP-citrate lyase (ACL) is the key enzyme responsible for decomposing citrate into acetyl-CoA for lipid generation. We estimated an ACL flux of 0.55 μmol/10^6 cells/day during Early Exponential phase. Since the G6PDH flux is less than 10% of ACL flux during this period, another pathway must be primarily responsible for generating NADPH for growth. This could be attributed to NADP-dependent isoforms of malic enzyme or isocitrate dehydrogenase (refer to Cataplerosis and Anaplerosis Section).

Flux into oxPPP, via G6PDH, reached its peak during Late Exponential and Stationary phases. NADPH/$NADP^+$ ratios fell during these phases (Fig. 5A), suggesting that the increase in oxPPP activity was possibly an adaptive response to reduced NADPH/$NADP^+$ levels (Hamanaka and Chandel, 2011). However, the upregulation of oxPPP flux was not sufficient to completely restore NADPH/

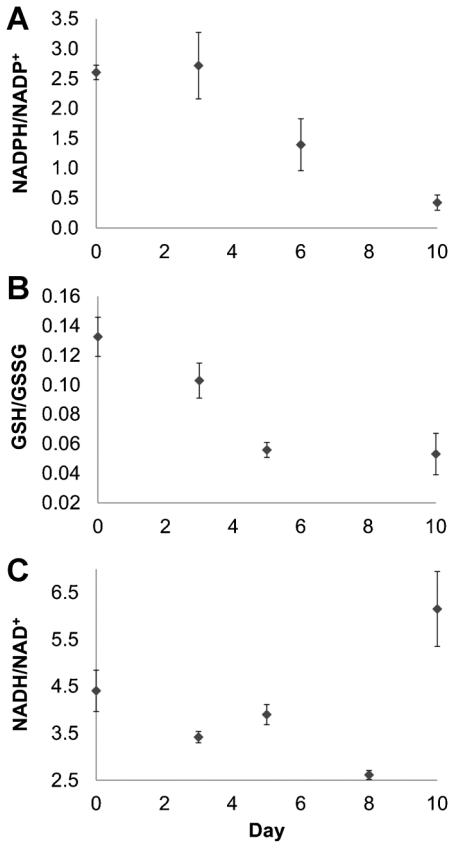

Figure 5. Intracellular redox ratios. **A**. Ratio of NADPH to $NADP^+$ as a function of time. **B**. Ratio of reduced (GSH) to oxidized (GSSG) glutathione. **C**. Ratio of NADH to NAD^+.

$NADP^+$ ratios to the levels observed during Early Exponential phase. The GSH/GSSG (reduced/oxidized glutathione) ratio (Fig. 5B) followed a similar trend, which can be explained by the fact that NADPH is the primary reductant molecule required to convert GSSG into GSH. Given that GSH is a major antioxidant molecule that functions to detoxify intracellular reactive oxygen species (ROS), it is possible that increased oxidative metabolism during Late Exponential and Stationary phases (see TCA Cycle Section below) was a source of enhanced ROS production, which triggered upregulation of oxPPP as an adaptive response to suppress oxidative stress (Sengupta and Morgan, 2010). Alternatively, glutathione plays a role in disulfide bond formation (Chakravarthi et al., 2006) and consequently protein folding, and the secretory machinery of CHO cells requires continuous NADPH-dependent remodeling of lipid membranes. Therefore, the observed increase in oxPPP flux could have been a direct response to increased antibody synthesis and secretion. In fact, a parallel study found evidence of elevated palmitate turnover during Stationary phase (Dean and Reddy, 2013), which provides some context in support of this latter possibility.

TCA Cycle

With a significant pyruvate flux routed into lactate during Early Exponential phase, little remained to be transported into mitochondria for oxidation. A parallel study found that multiple TCA metabolites derived substantial carbon from glutamine and asparagine during this period, leading to nearly half of the lipogenic palmitate being derived from these two amino acids (Dean and Reddy, 2013). Of the three NADH-producing dehydrogenase reactions in the TCA cycle, one of the three (malate dehydrogenase) was running in reverse, meaning that NADH was being consumed rather than generated. Therefore, in spite of substantial glutaminolysis, there was minimal NADH production associated with TCA cycle activity during Early Exponential phase. This result along with the high rate of lactate production indicates that minimal oxidative phosphorylation was taking place. Conversely, incoming flux to the TCA cycle from glycolysis peaked during Late Exponential and Stationary phases, which coincided with a decrease in the overall $NADH/NAD^+$ ratio (Fig. 5C). The fact that the $NADH/NAD^+$ ratio decreased most rapidly during Stationary phase, in spite of maximal TCA cycling, is indication of substantial oxidative activity during this phase. Even in the Decline phase, absolute fluxes associated with TCA cycling were maintained at higher levels than during Early Exponential phase. This is even more impressive considering that the total incoming carbon flux was reduced by almost two-thirds (Fig. 3).

One common trend across all phases was the correlation between oxPPP and TCA cycle fluxes. In general when oxPPP flux was minimal, TCA cycle flux was also minimal and vice versa. One potential explanation for this trend could involve the role of NADPH in neutralizing mitochondrial-derived reactive oxygen species (ROS) through maintenance of reduced glutathione levels (Sengupta and Morgan, 2010; Vander Heiden et al., 2009). ROS accumulation can lead to cell toxicity due to oxidation of cellular lipids, protein, and DNA (Halliwell, 2003; Scherz-Shouval and Elazar, 2007). Therefore, increasing oxPPP flux could be an adaptive response to enhance antioxidant capacity in the presence of high mitochondrial activity.

It is interesting, however, that oxPPP flux peaks at an earlier phase than TCA cycle flux. This could be attributed to two factors. First, the substantial drop in GSH/GSSG and $NADPH/NADP^+$ during Late Exponential phase (Fig. 5) may have triggered a compensatory increase in oxPPP to maintain redox homeostasis prior to the peak in TCA cycle flux. As discussed in the previous section, this could reflect increasing demand for NADPH to support antibody synthesis and secretion. Second, the substantial reduction in net specific growth rate from Late Exponential to Stationary phase may have decreased the NADPH demand for biosynthesis and therefore caused a reduction in overall oxPPP flux despite the continued decline in GSH/GSSG and $NADPH/NADP^+$ ratios.

Antibody Production

One significant result of our study was that increased antibody production (Fig. 1B) was closely associated with oxidative TCA cycle metabolism and oxPPP flux. To our knowledge, this is the first MFA study to examine this relationship between oxidative metabolism and antibody production. Through comparison of four separate phases of the fed-batch process, we observed a positive correlation between antibody production and oxidative TCA cycle flux, as indicated by the total flux through the CO_2-producing reactions of ADH, IDH, and PDH (Fig. 6). On the other

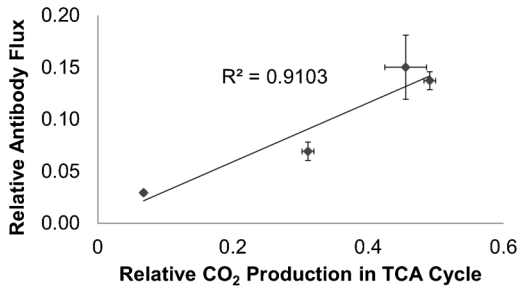

Figure 6. Correlation between oxidative TCA cycle flux and antibody production. Each point represents a separate phase of the fed-batch process, with TCA cycle and antibody fluxes normalized to the corresponding total incoming carbon flux reported in Figure 3. Oxidative TCA cycle flux was calculated by summing the rates of all three CO_2-producing TCA cycle reactions: PDH, IDH, and ADH. Error bars indicate standard errors.

hand, peak growth corresponded with peak glycolytic flux but minimal oxidative metabolism. Based upon our results, metabolic engineering to increase flux to TCA cycle during production phase has potential to enhance rates of specific antibody formation. Additional steps may be required to simultaneously divert more flux into oxPPP in order to maintain redox homeostasis and avoid toxic ROS accumulation. It is important to note, however, that TCA cycle activity was not independently varied in this study. Therefore, the correlation between antibody production and TCA cycle activity could be driven by some additional factor, such as intracellular redox status.

Cataplerosis and Anaplerosis

During Early Exponential phase, substantial flux was diverted into mitochondrial cataplerotic and anaplerotic pathways. Conversely, there was a large reduction in these fluxes during subsequent growth phases. During Early Exponential phase, ATP-citrate lyase (ACL) accounted for more than 75% of the flux leaving the citrate node. In another prior MFA study, ACL was determined to be a negligible flux during exponential phase (Ahn and Antoniewicz, 2011). However, our work used a serum-free medium without substantial fatty acid content, so cell growth required de novo lipid synthesis that in turn relied on ACL to supply AcCoA building blocks.

Substantial malic enzyme (ME) flux was also observed during Early Exponential phase, and although there was a large uncertainty associated with this value, closer examination of the 95% confidence interval reveals that even the lower 95% confidence bound of 1.3 μmol/10^6 cells/day is high in comparison to most other fluxes estimated during this growth phase. Like ME, phosphoenolpyruvate carboxykinase (PEPCK) could also be contributing cataplerotic flux from the TCA cycle to glycolysis; however, we cannot distinguish between these two pathways based upon our isotopomer measurements and have therefore lumped them together. ME in combination with anaplerotic PC flux effectively create a separate cycle overlapping with the TCA cycle. PC was found to have substantial flux during Early Exponential phase, returning much of the pyruvate generated by ME to the TCA cycle. PC can often be ignored in quiescent cells, but can carry a substantial flux in growing cultures (Hyder et al., 1996). Our analysis determined that the PC flux was at least as significant as pyruvate dehydrogenase (PDH) for channeling pyruvate into the TCA cycle during the initial growth period. The activity of PC was independently confirmed in a separate experiment using [1-^{13}C] pyruvate, the results of which can be found in the Supplementary Materials.

The high cycling through ME and PC could potentially explain the minimal oxPPP activity during Early Exponential phase, as NADP-dependent ME isoforms could have supplied the majority of cellular NADPH demands and thereby made additional oxPPP flux unnecessary. However, all three ME isoforms are known to exist in CHO cells (Hammond et al., 2011) and our MFA results cannot distinguish between them. Activity of the NADP-dependent ME1 isoform was confirmed for this study (results not shown), but results were inconclusive regarding the activities of ME2 and ME3. Therefore, it is difficult to state which isoform, if any, was dominant in catalyzing conversion of malate to pyruvate. Lastly, in addition to ME, isocitrate dehydrogenase (IDH) is also capable of producing NADPH. In general, the presence of multiple isoforms of both IDH and ME make it difficult to determine their contribution to the overall NAD(P)H production rates based on our MFA results.

Conclusions

As CHO cells transition from peak growth to peak antibody production, cell metabolism can change considerably over the course of a typical industrial fed-batch bioprocess. We aimed to quantify these global metabolic alterations using isotope labeling experiments and metabolic flux analysis. We found that high glycolytic flux positively correlated with peak growth, and specific lactate production was highest when specific growth rate was also highest. On the contrary, a highly oxidative state of metabolism was associated with increased antibody production, a result that, to our knowledge, has not been previously reported based on MFA studies. During peak specific antibody production (i.e., during Stationary phase), TCA cycling was at its maximum and lactate production was at its minimum. In fact, lactate was not produced at all, but instead was consumed. Furthermore, high oxidative pentose phosphate pathway flux was found to positively correlate with high TCA cycling and antibody production. This suggests that promoting oxidative TCA cycle metabolism and pentose phosphate pathway flux may provide a possible strategy to increase specific antibody production and reduce lactate accumulation during the production phase of industrial fed-batch CHO cell cultures.

The authors of this work have no pertinent conflicts of interest to report. Funding for this project was provided by Amgen Contract # 2010529686. Amgen also provided funding support for Jason Dean's postdoctoral training. The authors would like to thank all the Amgen analysts involved in this work; especially to Sheila Kingrey-Grebe for amino acid analysis, Jennifer Kerr for GC–MS set up, Louiza Dudin, Rajnita Charan, and Sumana Dey for cell culture media, and Angie Ziebart for mAb titer measurements.

Nomenclature

3PG	3-Phosphoglycerate
AcCoA	Acetyl-CoA
ACL	ATP Citrate Lyase
aKG	α-Ketoglutarate

Ala	Alanine
AMBIC	Ammonium bicarbonate
Arg	Arginine
Asp	Aspartate
ATP	Adenosine-5′-triphosphate
CHO	Chinese hamster ovary
Cit	Citrate
DHAP	Dihydroxyacetone phosphate
E4P	Erythrose-4-phosphate
F6P	Fructose-6-phosphate
Fum	Fumarate
G6P	Glucose-6-phosphate
G6PDH	Glucose-6-phosphate Dehydrogenase
GAP	Glyceraldehyde-3-phosphate
GC-MS	Gas chromatography–mass spectrometry
Glc	Glucose
Gln	Glutamine
Glu	Glutamate
GSH	Reduced gluathione
GSSG	Oxidzed glutathione
HK	Hexokinase
HPLC	High performance liquid chromatography
Lac	Lactate
mAb	Monoclonal antibody
Mal	Malate
ME	Malic enzyme
MFA	Metabolic flux analysis
MOX	Methoxyamine
MTBSTFA	*N*-methyl-*N*-(t-butyldimethylsilyl) trifluoroacetamide
NADH	Nicotinamide adenine dinucleotide
NADPH	Nicotinamide adenine dinucleotide phosphate
OAA	Oxaloacetate
PC	Pyruvate carboxylase
PEP	Phosphoenolpyruvate
oxPPP	Oxidative pentose phosphate pathway
Pro	Proline
Pyr.e	Extracellular pyruvate
Pyr	Pyruvate
R5P	Ribose-5-phosphate
ROS	Reactive oxygen species
RPM	Revolutions per minute
Ru5P	Ribulose-5-phosphate
S7P	Sedoheptulose-7-phosphate
Suc	Succinate
TBDMCS	Tert-butyldimethylchlorosilane
TCA Cycle	Tri-carboxylic acid cycle
VCD	Viable cell density
X5P	Xylulose-5-phosphate

References

Ahn WS, Antoniewicz MR. 2011. Metabolic flux analysis of CHO cells at growth and non-growth phases using isotopic tracers and mass spectrometry. Metab Eng 13(5):598–609. Elsevier. DOI: 10.1016/j.ymben.2011.07.002

Ahn WS, Antoniewicz MR. 2012. Towards dynamic metabolic flux analysis in CHO cell cultures. Biotechnol J 7(1):61–74. DOI: 10.1002/biot.201100052

Altamirano C, Paredes C, Illanes A, Cairó JJ, Gòdia F. 2004. Strategies for fed-batch cultivation of t-PA producing CHO cells: Substitution of glucose and glutamine and rational design of culture medium. J Biotechnol 110(2):171–179. DOI: 10.1016/j.jbiotec.2004.02.004

Altamirano C, Illanes A, Becerra S, Cairó JJ, Gòdia F. 2006. Considerations on the lactate consumption by CHO cells in the presence of galactose. J Biotechnol 125(4):547–556. DOI: 10.1016/j.jbiotec.2006.03.023

Antoniewicz MR, Kelleher JK, Stephanopoulos G. 2006. Determination of confidence intervals of metabolic fluxes estimated from stable isotope measurements. Metab Eng 8(4):324–337. DOI: 10.1016/j.ymben.2006.01.004

Antoniewicz MR, Kelleher JK, Stephanopoulos G. 2007. Elementary metabolite units (EMU): A novel framework for modeling isotopic distributions. Metab Eng 9(1):68–86. DOI: 10.1016/j.ymben.2006.09.001

Birch JR, Racher AJ. 2006. Antibody production. Adv Drug Deliv Rev 58(5–6):671–685. DOI: 10.1016/j.addr.2005.12.006

Bonarius HPJ, Timmerarends B, de Gooijer CD, Tramper J. 1998. Metabolite-balancing techniques vs. ^{13}C tracer experiments to determine metabolic fluxes in hybridoma cells. Biotechnol Bioeng 58: 258–262. DOI: 10.1002/(SICI)1097-0290(19980420)58:2/3<258::AID-BIT20>3.0.CO;2-7

Chakravarthi S, Jessop CE, Bulleid NJ. 2006. The role of glutathione in disulphide bond formation and endoplasmic-reticulum-generated oxidative stress. EMBO Rep 7(3):271–275. DOI: 10.1038/sj.embor.7400645

Dean J, Reddy P. 2013. Metabolic analysis of antibody producing CHO cells in fed batch production. Biotechnol Bioeng. DOI: 10.1002/bit.24826

Dean JT, Tran L, Beaven S, Tontonoz P, Reue K, Dipple KM, Liao JC. 2009. Resistance to diet-induced obesity in mice with synthetic glyoxylate shunt. Cell Metab 9(6):525–536. Elsevier Ltd. DOI: 10.1016/j.cmet.2009.04.008

DeBerardinis RJ, Mancuso A, Daikhin E, Nissim I, Yudkoff M, Wehrli S, Thompson CB. 2007. Beyond aerobic glycolysis: Transformed cells can engage in glutamine metabolism that exceeds the requirement for protein and nucleotide synthesis. Proc Natl Acad Sci USA 104(49): 19345–19350. DOI: 10.1073/pnas.0709747104

DeBerardinis RJ, Lum JJ, Hatzivassiliou G, Thompson CB. 2008. The biology of cancer: Metabolic reprogramming fuels cell growth and proliferation. Cell Metab 7(1):11–20. DOI: 10.1016/j.cmet.2007.10.002

Deshpande R, Yang TH, Heinzle E. 2009. Towards a metabolic and isotopic steady state in CHO batch cultures for reliable isotope-based metabolic profiling. Biotechnol J 4(2):247–263. DOI: 10.1002/biot.200800143

Dietmair S, Timmins NE, Gray PP, Nielsen LK, Krömer JO. 2010. Towards quantitative metabolomics of mammalian cells: Development of a metabolite extraction protocol. Anal Biochem 404(2):155–164. Elsevier Inc. DOI: 10.1016/j.ab.2010.04.031

Dorai H, Kyung YS, Ellis D, Kinney C, Lin C, Jan D, Moore G, Betenbaugh MJ. 2009. Expression of anti-apoptosis genes alters lactate metabolism of Chinese Hamster Ovary cells in culture. Biotechnol Bioeng 103(3):592–608. DOI: 10.1002/bit.22269

Fogolín MB, Wagner R, Etcheverrigaray M, Kratje R. 2004. Impact of temperature reduction and expression of yeast pyruvate carboxylase on hGM-CSF-producing CHO cells. J Biotechnol 109(1–2):179–191. DOI: 10.1016/j.jbiotec.2003.10.035

Folch J, Lees M, Stanley GHS. 1957. A simple method for the isolation and purification of total lipids from animal tissues. J Biol Chem 226(1):497–509. DOI: 10.1684/san.2011.0240

Follstad BA, 2012. Oxygen uptake rates in bioreactors. Personal Commun.

Glacken MW, Adema E, Sinskey AJ. 1988. Mathematical descriptions of hybridoma culture kinetics: I. Initial metabolic rates. Biotechnol Bioeng 32:491–506. DOI: 10.1002/bit.260320412

Goudar CT, Biener R, Konstantinov KB, Piret JM. 2009. Error propagation from prime variables into specific rates and metabolic fluxes for

mammalian cells in perfusion culture. Biotechnol Progr 25(4):986–998. DOI: 10.1021/bp.155

Goudar C, Biener R, Boisart C, Heidemann R, Piret J, de Graaf A, Konstantinov K. 2010. Metabolic flux analysis of CHO cells in perfusion culture by metabolite balancing and 2D [^{13}C, ^{1}H] COSY NMR spectroscopy. Metab Eng 12(2):138–149. DOI: 10.1016/j.ymben.2009.10.007

Halliwell B. 2003. Oxidative stress in cell culture: An under-appreciated problem? FEBS Lett 540(1–3):3–6. DOI: 10.1016/S0014-5793(03)00235-7

Hamanaka RB, Chandel NS. 2011. Warburg effect and redox balance. Science 334:1219–1221.

Hammond S, Kaplarevic M, Borth N, Betenbaugh MJ, Lee KH. Chinese Hamster Genome Database: An Online Resource for the CHO Community at www.CHOgenome.org. Biotechnology and Bioengineering 2011. DOI: 10.1002/bit.24374

Hansen HA, Emborg C. 1994. Influence of ammonium on growth, metabolism, and productivity of a continuous suspension Chinese hamster ovary cell culture. Biotechnol Progr 10(1):121–124. DOI: 10.1021/bp00025a014

Hyder F, Chase JR, Behart KL, Mason GF, Siddeek M, Rothmans DL, Shulman RG. 1996. Increased tricarboxylic acid cycle flux in rat brain during forepaw stimulation detected with ^{1}H [^{13}C] NMR. Biophysics 93(July):7612–7617.

Li J, Wong CL, Vijayasankaran N, Hudson T, Amanullah A. 2012. Feeding lactate for CHO cell culture processes: Impact on culture metabolism and performance. Biotechnol Bioeng 109(5):1173–1186. DOI: 10.1002/bit.24389

Metallo CM, Walther JL, Stephanopoulos G. 2009. Evaluation of ^{13}C isotopic tracers for metabolic flux analysis in mammalian cells. J Biotechnol 144(3):167–174. DOI: 10.1016/j.jbiotec.2009.07.010

Möllney M, Wiechert W, Kownatzki D, de Graaf AA. 1999. Bidirectional reaction steps in metabolic networks: IV. Optimal design of isotopomer labeling experiments. Biotechnol Bioeng 66(2):86–103.

Nolan RP, Lee K. 2011. Dynamic model of CHO cell metabolism. Metab Eng 13(1):108–124. Elsevier. DOI: 10.1016/j.ymben.2010.09.003

Nyberg GB, Balcarcel RR, Follstad BD, Stephanopoulos G, Wang DI. 1999. Metabolism of peptide amino acids by Chinese hamster ovary cells grown in a complex medium. Biotechnol Bioeng 62(3):324–335.

Omasa T, Higashiyama K, Shioya S, Suga K. 1992. Effects of lactate concentration on hybridoma culture in lactate-controlled fed-batch operation. Biotech Bioeng 39(5):556–564. DOI: 10.1002/bit.260390511

Ozturk SS, Palsson BO. 1990. Chemical decomposition of glutamine in cell culture media: Effect of media type, pH, and serum concentration. Biotechnol Progr 6(2):121–128. DOI: 10.1021/bp00002a005

Quek L-E, Dietmair S, Krömer JO, Nielsen LK. 2010. Metabolic flux analysis in mammalian cell culture. Metab Eng 12(2):161–171. DOI: 10.1016/j.ymben.2009.09.002

Sauer U. 2006. Metabolic networks in motion: ^{13}C-Based flux analysis. Mol Syst Biol 2:62. DOI: 10.1038/msb4100109

Scherz-Shouval R, Elazar Z. 2007. ROS, mitochondria and the regulation of autophagy. Trends Cell Biol 17(9):422–427. DOI: 10.1016/j.tcb.2007.07.009

Sellick CA, Hansen R, Maqsood AR, Dunn WB, Stephens GM, Goodacre R, Dickson AJ. 2009. Effective quenching processes for physiologically valid metabolite profiling of suspension cultured mammalian cells. Anal Chem 81(1):174–183. DOI: 10.1021/ac8016899

Sengupta N, Rose ST, Morgan JA. 2011. Metabolic flux analysis of CHO cell metabolism in the late non-growth phase. Biotechnol Bioeng 108(1):82–92. DOI: 10.1002/bit.22890

Seth G, Hossler P, Chong J, Hu YW. 2006. Engineering cells for cell culture bioprocessing–physiological fundamentals. Chem Eng 101(June):119–164. DOI: 10.1007/10_017

Shaw RJ. 2006. Glucose metabolism and cancer. Curr Opin Cell Biol 18(6):598–608. DOI: 10.1016/j.ceb.2006.10.005

Sheikh K, Fo J, Nielsen LK. 2005. Modeling hybridoma cell metabolism using a generic genome-scale metabolic model of mus musculus. Biotechnol Progr 21(1):112–121. DOI: 10.1021/bp0498138

Smoot ME, Ono K, Ruscheinski J, Wang PL, Ideker T. 2011. Cytoscape 2.8: new features for data integration and network visualization. Bioinformatics 27(3):431–432. DOI: 10.1093/bioinformatics/btq675

Vander Heiden MG, Cantley LC, Thompson CB. 2009. Understanding the Warburg effect: The metabolic requirements of cell proliferation. Science (New York, N.Y.) 324(5930):1029–1033. DOI: 10.1126/science.1160809

Xie L, Wang DIC. 1996. Energy metabolism and ATP balance in animal cell cultivation using a stoichiometrically based reaction network. Biotechnol Bioeng 52:591–601. DOI: 10.1002/(SICI)1097-0290(19961205)52:5<591

Xing Z, Kenty B, Koyrakh I, Borys M, Pan S-H, Li ZJ. 2011. Optimizing amino acid composition of CHO cell culture media for a fusion protein production. Process Biochem 46(7):1423–1429. Elsevier Ltd. DOI: 10.1016/j.procbio.2011.03.014